

A NOVEL MICROMILLING TECHNOLOGY BASED ON SINGLE-POINT TOOL TIP GEOMETRY

Eberhard Bamberg, Sumet Heamawatanachai
Precision Design Laboratory, Department of Mechanical Engineering
University of Utah
Salt Lake City, UT, USA

INTRODUCTION

To machine increasingly smaller features with defined geometry tools such as end mills, manufacturing the tool becomes increasingly more difficult. This is due to the complex geometry of end mills which typically involve two or more helical flutes on the outside diameter of the tool. The flutes, which are difficult to make to begin with, reduce the stress carrying cross section of the end mill, thereby increasing the likelihood of tool breakage, especially for very small tool diameters of 0.2 mm and less [1]. Also, it has been observed that micro end mills are prone to chip clogging, which then leads to breakage of the tool [2]. The novel micromilling technique presented in this paper has elements similar to ultrasonic face milling [3], yet its cutting mechanism is based on a single-point tool-material interaction, which is very different from anything existing. The reduced stresses from single-point tools compared to standard cylindrical tools has been shown in diamond turning to enable ductile material removal of otherwise brittle materials such as silicon [4-5]. This greatly increases the surface quality to the mirror-type surface finish that diamond turning is known for.

CUTTING MODULE

This novel micromilling technology is based on single-point diamond tip milling which can be used to machine micro-sized features into a wide range of materials ranging from polymers, through metals to glass. The unique characteristic of this technology is that the cutting velocity is not created by rotating the tool tip about its axis of rotation. Instead, the cutting motion is generated by actuating the tool tip on a recirculating, microscopic trajectory at high frequencies. This allows a standard 3-axis setup to generate the macroscopic motion required for the tool path while at the microscopic level, the cutting motion and the tool tip path are being generated by the tool itself. As a result, truly three-dimensional

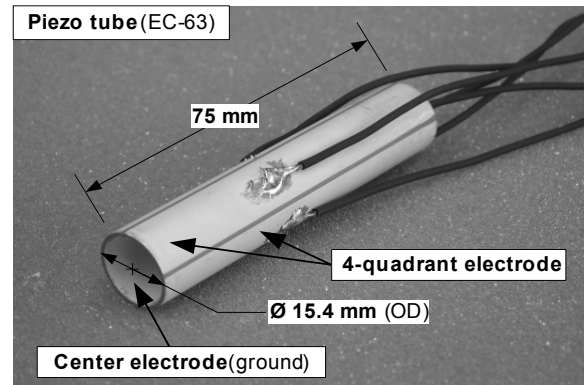


FIGURE 1. The ceramic piezo tube scanner (PZT) with four electrodes on the outside surface and the center ground on the inside surface.

part geometries at the micron level with exceptional surface finish and part accuracy can be created.

The microscopic motion of the tool tip is achieved by a 75 mm long piezo tube scanner (PZT) shown in FIGURE 1.) and is made from EC-63 ceramics with an outer diameter of 15.4 mm and a wall thickness of 0.79 mm with four external electrodes. By energizing the four electrodes with time-varying voltages that range between 0 and -1000 V, periodic bending of the free end of the tube is achieved. If the voltages are sinusoidal with a phase lag of 90 degrees between adjacent electrodes, the resulting periodic bending creates a planar, orbiting motion with a maximum radius of 35 μm that is perpendicular to the PZT's axis.

The concept of the voltage generation is shown in FIGURE 2.) and consists of a National Instruments DAQ card (PXI-6040E) and four high-voltage piezo amplifiers (PI E-507.00) which amplify the 0 - 10 V analog waveforms by a factor of minus 100 to produce the 0 to -1000 V used to drive the PZT.

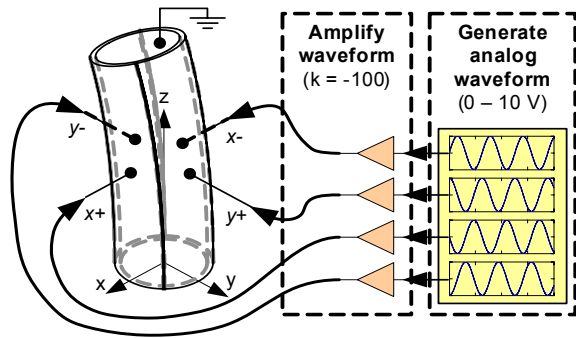


FIGURE 2. The PZT is actuated by analog voltages that vary from 0 to -1000 V.

Since the orbiting motion is planar, the machined surface is flat, making this cutting mode the equivalent of a miniaturized fly cutter, whose tool tip offset from the axis of rotation can be varied during cutting simply by varying the amplitude of the driving voltages (FIGURE 3.).

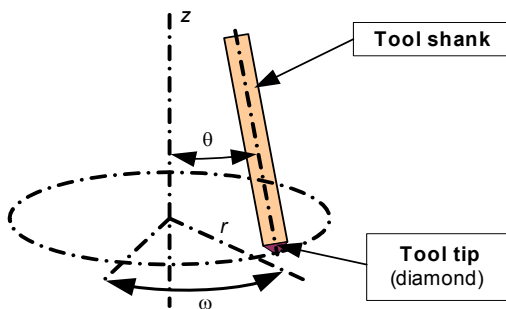


FIGURE 3. The cyclic bending of the PZT generates a planar, orbital motion similar to a fly cutter.

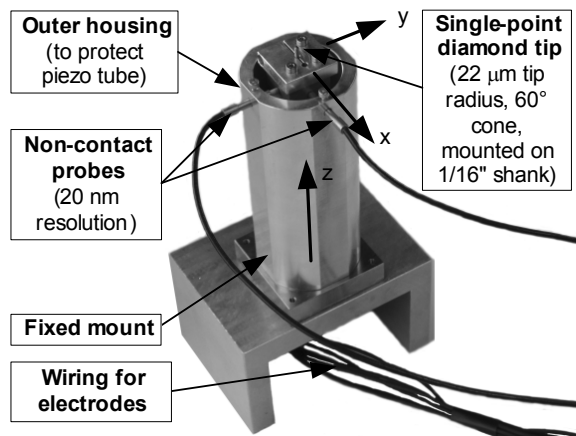


FIGURE 4. The cutting module prototype consists of the PZT, a housing to protect the tube, a clamp to hold the tool shank, and non-contact probes to monitor the cutting motion.

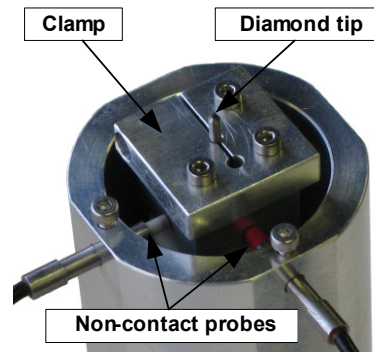


FIGURE 5. A clamp holding the tool shank is mounted to the free end of the PZT.

TOOL PATHS

While applying properly timed sinusoidal voltages creates cyclic bending that will result in a circular orbiting motion of the free end (FIGURE 3.), other modes of actuation are possible as well. For example, the magnitude of the x- and y voltages can be varied as shown in EQ. (1), resulting in different amplitudes in both directions. This would lead to an elliptical tool path as shown in FIGURE 6.).

$$\begin{aligned}
 x+ &= V_{1x} \sin(\omega t) \\
 x- &= V_{1x} \sin(\omega t + \pi) \\
 y+ &= V_{1y} \cos(\omega t) \\
 y- &= V_{1y} \cos(\omega t + \pi)
 \end{aligned}
 \tag{EQ. (1)}$$

Even more complex tool paths can be generated if the length of the tube is manipulated as well. For example, the length of the tube can be shortened or lengthened by applying the same voltage to all four electrodes. This causes the tool to change its position in the z-axis (the height). Overlaying such a voltage on top of the primary voltage then causes orbiting of the tool tip while simultaneously allowing its height to be changed. The voltage that is applied to manipulate the

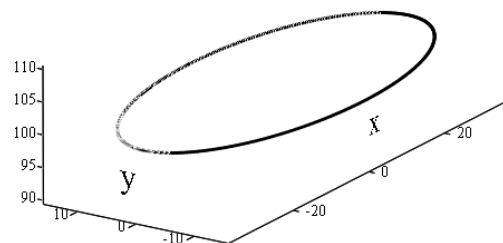


FIGURE 6. Plane, elliptic motion as a result of voltages shown in EQ. (1).

length of the PZT tube is referred to as the secondary voltage V_2 .

$$\begin{aligned} x+ &= V_1 \sin(\omega t) + V_2 \cos(\omega t + \varphi) \\ x- &= V_1 \sin(\omega t + \pi) + V_2 \cos(\omega t + \varphi) \\ y+ &= V_1 \cos(\omega t) + V_2 \cos(\omega t + \varphi) \\ y- &= V_1 \cos(\omega t + \pi) + V_2 \cos(\omega t + \varphi) \end{aligned} \quad \text{EQ. (2)}$$

The sinusoidal secondary voltage V_2 in EQ. (2) causes a tilt of the orbiting motion. The orientation is determined by the phase lag φ . For $\varphi=0$, the tilt will be about the y-axis while $\varphi=90^\circ$ results in tilt about the x-axis (FIGURE 7.).

The resulting tilted motion allows tapered surfaces to be machined without the need for tilting the work piece (or the spindle) or the use of a tapered end mill. The tilt angle is easily adjustable by varying the magnitude of the secondary voltage while the orientation of the tilt with respect to the z-axis is easily adjusted by the phase lag φ in the secondary voltages V_2 .

CONTROL

The analog voltages that drive the PZT are generated with a National Instruments card that is controlled by LabVIEW. The card used for the prototype only has two analog channels which produce two sinusoidal waveforms with a 90° phase. These voltages drive the x+ and y+ electrodes. To generate the voltages required to power the x- and y- electrodes, a separate circuit with op-amps was used to invert the voltages, thereby creating the required 180° phase between the positive and negative electrodes such that the x-axis electrodes are driven by the same voltage but with a 180° phase lag. The LabVIEW control VI is shown in FIGURE 8.) and

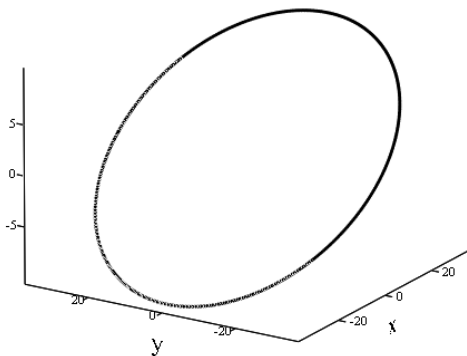


FIGURE 7. Orbiting motion tilted about the x-y plane as a result of voltages shown in EQ. (2).

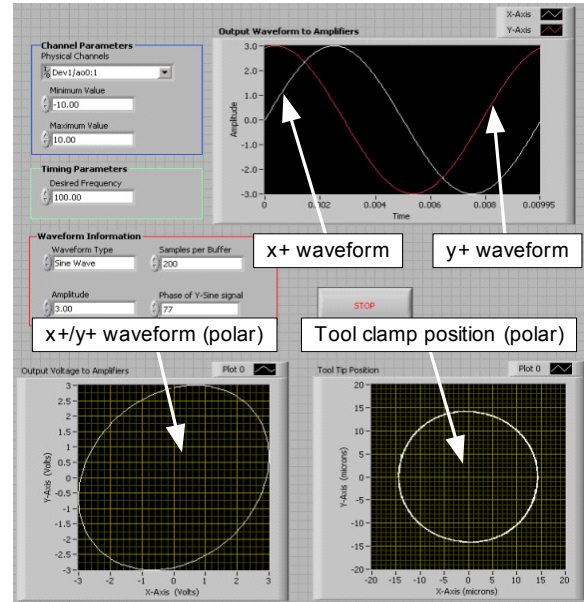


FIGURE 8. LabVIEW VI showing the two sinusoidal waveforms for the two positive electrodes and the resulting motion of the tool clamp.

illustrates the two sinusoidal waveforms that generate the driving voltage for the two positive PZT electrodes, x+ and y+. Also shown is the circular motion of the tool clamp as measured by the non-contact probes.

From FIGURE 8.) it is interesting to note, that the polar plots of the x+/y+ waveform and the resulting tool motion don't match. While the tool motion is clearly circular, the driving voltage to generate this motion is shaped like an oval with a phase of 77° between the two waveforms. This is most likely the result of manufacturing and assembly tolerances but also due to variations in material properties of the PZT itself.

MACHINING EXPERIMENTS

To demonstrate the machining ability of the prototype, the cutting module was mounted on a 3-axis micro-EDM machine (Optimization Profile 24P) that is equipped with an x-y stage that is driven by piezoelectric linear motors and encoders with a resolution of 100 nm. Five different materials in the form of flat stock were machined. These were: acrylic (polycarbonate), pure copper, stainless steel (304), titanium-alloy (Ti-6Al-4V), and glass. A 2-1/2-D tool path was programmed to machine a microfluidic-type feature with outer dimensions of 450×450 microns. This feature milled into stainless steel to a depth of

15 μm is shown in FIGURE 9.) with a surface roughness of 0.138 μm R_a . The same feature machined in pure glass is shown in FIGURE 10.) with a comparable surface finish. Both features were machined at a feed rate of 5 $\mu\text{m}/\text{s}$, a depth of cut of 5 μm and a 10 μm step over between passes.

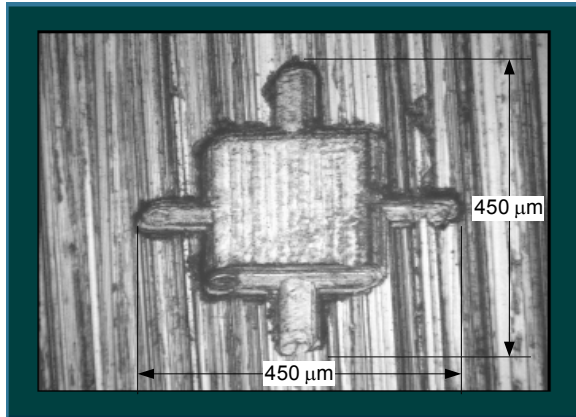


FIGURE 9. Intensity plot of microfluidic feature of size 450 x 450 μm in stainless steel.

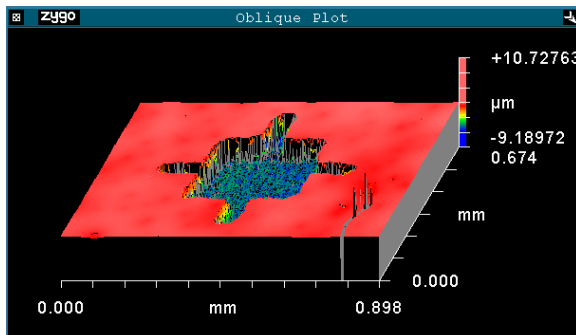


FIGURE 10. 3D view of microfluidic feature machined into glass. The surface roughness was measured as 0.184 μm .

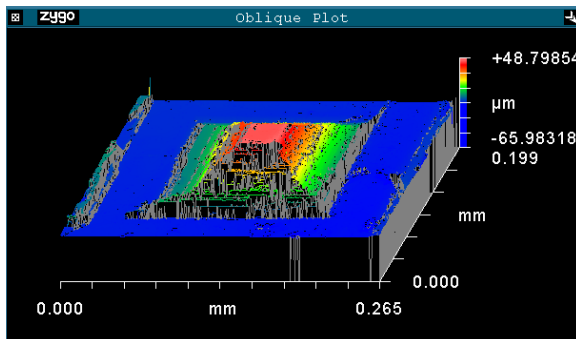


FIGURE 11. 100x100 μm pyramid with a height of 107 μm milled into pure copper. The R_a surface roughness of the machined bottom is 0.294 μm .

This was followed by a 3-dimensional tool path that cut a 100 x 100 micron pyramid with a total height of 100 microns in pure copper. FIGURE 11.) depicts a white light interferometer scan of the feature. The top surface (shown in red) is the material surface. The bottom of the pyramid is milled to a depth of 107 μm . The excellent R_a surface finish of less than 0.294 μm and the detailed shape of the pyramid are clearly visible.

CONCLUSIONS

This novel micromilling technique is based on single-point diamond tips that are actuated at the microlevel by a piezo tube scanner. The resulting tool tip paths, which are used to generate the cutting motion, have a maximum amplitude of 35 microns and a maximum frequency of 200 Hz. By actuating the tool tip on its own, recirculating tool paths, the cutting speed is decoupled from the feed speed, making this the equivalent of a miniature fly cutter. Machining experiments with ductile and brittle materials were conducted and the machined features showed excellent surface roughness and part accuracies. As a novel micromilling technique, this tool is intended for the prototyping of small parts in typically difficult to machine materials.

ACKNOWLEDGMENTS

The authors would like acknowledge the financial support by the University of Utah Seed Program.

REFERENCES

- [1] I. Tansel, O. Rodriguez, M. Trjillo, E. Paz, W. Li, "Micro-end-milling - I. Wear and Breakage", *International Journal of Machine Tool and Manufacture*, 38 (1998), pp. 1419-1436.
- [2] W. Koenig, K. Kutzner, U. Schehl, "Tool monitoring of small drills with acoustic emission", *International Journal of Machine Tool and Manufacture*, 32 (1992), pp. 487-493.
- [3] Z.J. Pei, P.M. Ferreira, "An experimental investigation of rotary ultrasonic face milling", *International Journal of Machine Tool and Manufacture*, 39 (1999), pp. 1327-1344.
- [4] P.S. Pizani, R. Jasinevecius, J.G. Duduch, A.J.V. Porto, "Ductile and brittle modes in single-point-diamond-turning of silicon probed by Raman scattering", *Journal of Materials Science Letters*, 18 (1999), pp. 1185-1187.
- [5] J.A. Patten, W. Gao, "Extreme negative angle technique for single point diamond nano-cutting of silicon", *Precision Engineering*, 25 (2001), pp. 165-167.